Structure of the Polymer Backbones in polyMOF Materials

Paulo G.M. Mileo,[1] Shichen Yuan,[2] Sergio Ayala Jr.,[3] Pu Duan,[2] Rocio Semino,[1] Seth M. Cohen,[3]* Klaus Schmidt-Rohr,[2]* and Guillaume Maurin[1]*

[1] ICGM, Univ. Montpellier, CNRS, ENSCM, Montpellier, France
[2] Department of Chemistry, Brandeis University, Waltham, MA 02453, USA
[3] Department of Chemistry and Biochemistry, University of California, San Diego, La Jolla, CA 92093 USA

ABSTRACT: The molecular connectivity of polymer metal-organic framework (polyMOF) hybrid materials was investigated using Density Functional Theory calculations and solid-state NMR spectroscopy. The architectural constraints that dictate formation of polyMOFs were assessed by examining poly(1,4-benzenedicarboxylic acid) (pbdc) polymers in two archetypical MOF lattices (UiO-66 and IRMOF-1). Modeling of the polyMOFs showed that in the IRMOF-1-type lattice 6, 7, and 8 methylene (-CH_2-) groups between 1,4-benzenedicarboxylate (bdc^{2-}) units can be accommodated without significant distortions, while in the UiO-66-type lattice, an optimal spacing of 7 methylene groups between bdc^{2-} units, is needed to minimize strain. Solid-state NMR supports these predictions, revealing pronounced spectral differences for the same polymer in the two polyMOF lattices. With 7 methylene groups, polyUiO-66-7a shows 7±3% of uncoordinated bdc^{2-} linkers, while uncoordinated bdc^{2-} linkers are undetectable (<4%) in the corresponding polyIRMOF-1-7a. In addition, NMR-detected backbone mobility is significantly higher in the polyIRMOF-1-7a than in the corresponding polyUiO-66-7a, again indicative of taut chains in the latter.

INTRODUCTION

The integration of metal-organic frameworks (MOFs) with polymers has inspired new composite materials that amplify the properties of the individual MOF or polymer components.[1-2] A continuum of MOF-polymer composites has been reported, including MOF-based mixed-matrix membranes (MMMs),[3-4] MOFs with polymers grafted on their surface,[5-7] MOF-templated polymers,[8-10] as well as polymer-templated MOFs.[11-12] With increasing complexity of these MOF-polymer composites, there is a need for improved characterization of the interface formed between MOFs and polymers. In this respect, many bulk characterization measurements have been reported using scanning electron microscopy (SEM),[13] dynamic mechanical analysis (DMA),[14] Raman spectroscopy,[15] and ultramicrotomy combined with transmission electron microscopy (TEM).[16] Molecular modeling and solid-state NMR (ssNMR) have been successfully coupled to gain molecular-level characterization of various MOF-polymer composites.[1] Kitagawa and coworkers combined ssNMR and molecular dynamics (MD) simulations to model the infiltration of polymers into the pores of 1D-channel MOFs.[17] They analyzed the conformations of the confined polymers[17] revealed their thermal transitions,[18] and characterized the separation of two non-interacting polymers in MOF pores.[19] Similarly, ssNMR and molecular modeling were used to investigate the MOF-polymer interface of MOF MMMs prepared from UiO-66 and either poly(vinylidene fluoride) (PVDF) or poly(ethylene oxide)(PEO).[20] This study revealed that while PVDF shows only surface contact with UiO-66, PEO is completely infiltrated into the pores of the MOF.[21] These examples illustrate that a subtle interplay of ssNMR and molecular simulations is highly relevant to characterize the interactions between the MOFs and the polymers despite the lack of molecular connectivity in these composites.

PolyMOFs are a unique class of hybrid materials wherein a synthetic polymer serves as a ligand to synthesize MOFs.[22] In contrast to the composites mentioned above, polyMOFs are hybrids at the molecular level, where 1-dimensional, amorphous polymers containing 1,4-benzenedicarboxylic acid (H_2bdc) linkers are used as the building blocks to construct 3-dimensional porous materials as shown schematically in Figure 1. Using a polymer ligand to synthesize polyMOFs has yielded materials with enhanced stability,[22-23] hierarchical porosity,[24] and controlled morphologies and crystal sizes.[11, 25] However, to generate polyMOFs, the molecular restraints of the MOF lattice and the linker spacing along the polymer backbone must be fulfilled simultaneously. Several reports have probed the polymer-MOF structure relationships in polyMOFs indirectly by varying the methylene (-$(CH_2)_x$-) spacer length in the backbone of the polymer.[22-24] Other studies on polyMOFs have examined the concept of isoreticular chemistry,[23, 26] the use of block co-polymers,[11, 25, 27] and have investigated different MOF architectures.[28]

Herein, a combination of Density Functional Theory (DFT) and ssNMR is used to elucidate the polymer structure within polyMOFs. PolyMOFs of IRMOF-1 and

UiO-66 were studied. These polyMOFs are comprised of linear poly(1,4-benzenedicarboxylic acid) (pbdc) polymer ligands that have H_2bdc units connected by $-(CH_2)_x-$ segments (Figure 1). The polyMOFs are denoted as either polyUiO-66-xa or polyIRMOF-1-xa, where 'x' represents the number of $-CH_2-$ groups between H_2bdc units, while 'a' denotes that the polymers contain carboxylic acid coordinating groups. DFT calculations described below suggest that while polyIRMOF-1 is able to conform the alkyl backbone spacer without distortions, polyUiO-66 is much less accommodating. ^{13}C and ^{1}H-^{13}C ssNMR measurements were performed and support the computational findings, as well as provide further insight into defects and dynamics of the polymeric backbone. Structural distortions caused by strained backbone segments between linkers in the lattice are reflected in additional chemical-shift variations. Defects within the MOFs are detected, including uncoordinated H_2bdc linkers. ssNMR was also used to distinguish slack from taut backbone segments of the polymer ligand within the pores of the polyMOF by detecting the effects of backbone mobility on anisotropic line broadening. This work features the first in- depth study of polyMOF structures on the segmental level and demonstrates that the combination of molecular modeling and ssNMR is a powerful approach for probing the structure and mobility of backbone and linker segments in polyMOFs.

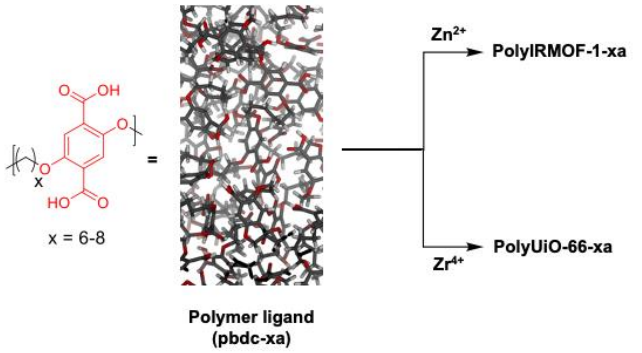

Figure 1. Representation of a pbdc-xa polymer and its monomers with H_2bdc units separated by $-(CH_2)_x-$ segments. These polymers form polyMOFs when combined with appropriate metal ions as denoted.

RESULTS AND DISCUSSION

As a first step in the modeling, the preferential arrangement of polymer ligands in the pores of IRMOF-1 was assessed by incorporating a single $-(CH_2)_x-$ chain (x = 6-8) in four different possible configurations (Figure S1). These structures were further geometry optimized at the DFT-level using the GGA/PBE functional[29] and D3 dispersion corrections[30] as implemented in the CP2K[31] code (see ESI for details). The most stable structure for each $-(CH_2)_x-$ segment length (x = 6-8) was determined by comparing the total electronic energies when the spacer is placed in these different configurations (Figure S2). Configuration 1, in which the spacer is connected to two adjacent bdc^{2-} linkers that are oriented perpendicular to one another, is favored in polyIRMOF-1-6a. Configuration 2, which corresponds to the spacer extended from across one face of the MOF lattice connecting opposite bdc^{2-} linkers, is preferred for polyIRMOF-1-7a and polyIRMOF-1-8a (Figure 2). Less favorable configurations of the alkyl spacers are shown in Figure S2b, in which the spacer extends diagonally across the pore of the MOF (Configuration 3), and wherein the spacer connects two orthogonally adjacent faces of IRMOF-1 (Configuration 4). Energy differences are quite pronounced when the spacers are not in their most stable configuration (up to 10^3 kJ mol^{-1}), but for x = 8, the energy differences between Configurations 1 and 2 or 2 and 3 differ by only 10 kJ mol^{-1} (Figure S2). The most stable spacer configurations for the polyIRMOF-1-xa series are depicted in Figure S3. Further analyses of the C-C bond lengths and C-C-C angles (Table S1) show that there are no significant differences in the strain suffered by the x = 6, 7, and 8 carbon spacers in all polyIRMOF-1, when the spacers are in their appropriate configurations (i.e., x = 6 is in Configuration 1, and x = 7, 8 are in Configuration 2, Figure 2). Overall, the models indicate that the polymer chains can be accommodated in the pores of IRMOF-1 with very limited mechanical constraints.

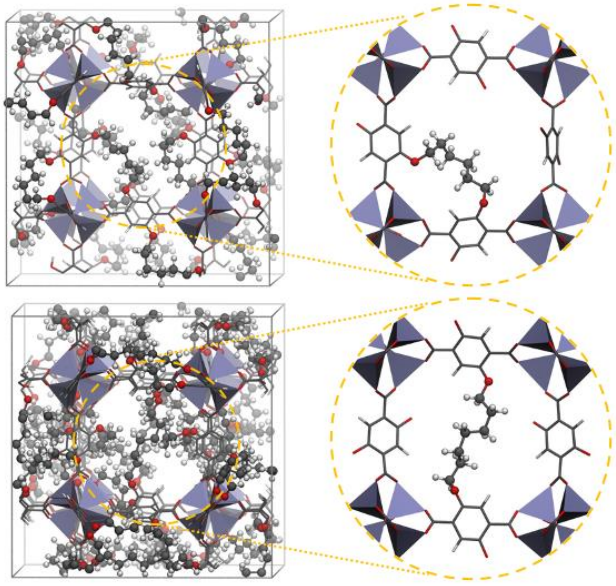

Figure 2. DFT minimum energy structures of the periodic polyIRMOF-1-6a (*top*) and polyIRMOF-1-7a (*bottom*) built from the assembly of Zn_4O nodes and pbdc polymer ligands. Color code: O (red), Zn (steel blue), C (gray), H (white).

The most stable single-chain configurations were further extended to build fully connected periodic polyIRMOF-1-xa structures, where all the bdc^{2-} linkers were considered

to be bridged with the backbone spacers. A non-uniform distribution of connecting groups has not been sampled here because it would require the consideration of large supercells computationally prohibitive at the DFT level. The corresponding structures for the cases of x = 6 and 7 are shown in Figure 2, while the polyIRMOF-1-8a model is shown in Figure S4. Notably, all DFT-optimized polyIRMOF-1-xa models show very similar cell dimensions to those of IRMOF-1 (Table S3). The polymer chains of these DFT-optimized structures are all connected by covalent bonds to the bdc^{2-} linkers and they do not exhibit significant distortions, consistent with the calculations performed on a single chain. The bulk of the methylene chains in the polyIRMOF-1-xa models results in a significant drop in pore accessibility (Table S4). Typically, the N_2 accessible surface area and free pore volume of polyIRMOF-1-8a both decrease by more than 50% (1550 m_2/g and 0.658 cm_3/g) when compared to IRMOF-1 (3770 m_2/g and 1.357 cm_3/g). This simulated trend is consistent with the reduction in the experimental N_2 BET area of polyIRMOF-1-8a previously reported (856 m_2/g vs 2963 m_2/g for IRMOF-1).[22]

We next examined UiO-66-based polyMOFs following the same procedure detailed above for the polyIRMOF-1-xa series. Because this MOF possesses two distinct cages, octahedral (O_h) and tetrahedral (T_g), both were considered as possible locations for the spacers, leading to the exploration of several configurations incorporating a single chain (Figures S5 and S6, respectively). As an example, several single-chain configurations in the O_h cage of polyUiO-66-7a are shown in Figure 3, with Figure 3b displaying the most stable configuration regardless of segment length. It was found that the arrangements of a single chain are much less energetically favorable in the T_g cages (Figure S7). Therefore, the most stable structures in the O_h cage were selected for further analyses (Figure S8).

Significant distortions were observed in terms of both C-C distances and C-C-C angles in the conformations of the $-(CH_2)_x-$ segments for the case of x = 6, while the geometric features of the chains for cases of x = 7 and 8 remained similar to those observed for polyIRMOF-1 (Tables S1 and S2). This indicates that the length of the x = 6 spacer is too short to connect the bdc^{2-} units without significant strain in polyUiO-66-6a. The fully connected periodic polyUiO-66 models were thus constructed and DFT-optimized. In stark contrast with the scenario encountered for polyIRMOF-1, the polyUiO-66 periodic structures were found to be unstable owing to the highly confined environment of their cages that imposes high mechanical constraints on the chains. This implies that not all the bdc^{2-} linkers maintain their connectivity in the DFT-optimized polyUiO-66 structures. This scenario is even much more pronounced for x = 6 (Figure S9), consistent with the higher degree of distortion of the $-(CH_2)_x-$ segments revealed on the single-chain configurations. This conclusion suggests that uncoordinated bdc^{2-} units can be anticipated in the case of polyUiO-66 materials.

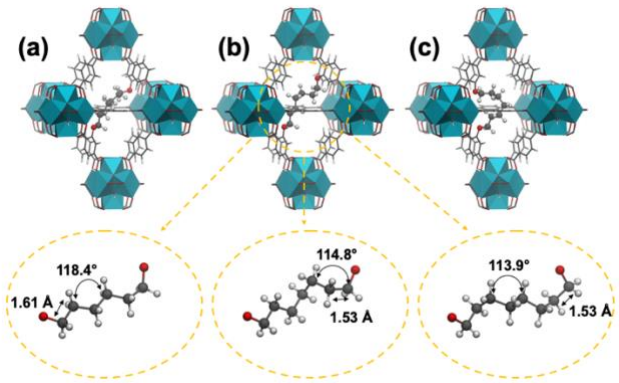

Figure 3. DFT-optimized single-chain configurations in the O_h cage of polyUiO-66-7a (*top*). Configuration b was shown to be the most stable one whatever the segment length. Bond angles and lengths of the methyl segments found for the DFT-optimized single-chain configurations polyUiO-66-xa (x = 6, 7, 8) for configuration b (*bottom*).

To validate the conclusions drawn from the modeled polyMOF structures and gain more insight into the defects and dynamics of the polymer backbone, the polyMOFs were synthesized and further characterized by ssNMR. The synthesis of the polymer ligands was adapted from previously published procedures.[22, 24] The average molecular weight M_n of the polymers ranged from 4400-4800 g/mol, the dispersity (M_w/M_n) of the polymers ranged between 1.4-1.9, and the degree of polymerization was 13-14 repeat units. Complete synthesis procedures and characterization can be found in the ESI.

Among the polyUiO-66-xa materials with x = 6-8, polyUiO-66-7a formed the most crystalline polyMOF structure with the largest crystallites, as gauged by powder X-ray diffraction (PXRD) (Figure S10) and scanning electron microscopy (SEM) (Figures S14-S16). These experimental results made polyUiO-66-7a the most attractive candidate for comparison with the DFT simulations. The other polyUiO-66-xa (x = 6, 8) materials showed poorer crystallinity, consistent with the added strain as observed computationally. Specifically, the PXRD of polyUiO-66-8a (Figure S10) displays very broad Bragg diffraction peaks that can be attributed to the presence of pervasive defects within the polyMOF lattice.[24] PXRD of polyUiO-66-6a shows appreciable crystallinity, but finite-size broadening of Bragg peaks and small crystals in SEM (Figures S10 and S14). Correspondingly, ssNMR of polyUiO-66-6a reveals that a significant amount of the H_2bdc units (20%) are uncoordinated and clustered (Figures S17-S19), qualitatively in line with the lattice disruptions in the calculations. Therefore, polyUiO-66-xa (x = 6 and 8) were not inspected by detailed evaluation using ssNMR.

All polyIRMOF-1-xa (x = 6-8) materials displayed appreciable crystallinity with a cubic morphology, as confirmed by PXRD (Figure S20) and SEM (Figures S24-

S26). For polyIRMOF-1-xa, all of the -$(CH_2)_x$- spacers could be accommodated without significant distortion, but ssNMR results revealed that polyIRMOF-1-7a is the most relaxed structure. By ssNMR, polyIRMOF-1-7a displayed the smallest ^{13}C NMR line widths (Figure S27), indicating the least static conformational disorder. PolyIRMOF-1-7a also exhibited the smallest ^{1}H line width (Figure S28) and -OCH_2- chemical-shift anisotropy (discussed later, see ESI for details), signifying the least constraints on segmental motions. NMR showed that conformational disorder and dynamic constraints in all the polyIRMOF-1 materials were less than those for the polyUiO-66 materials.

Based on the aforementioned observations, the ssNMR spectra of pbdc-7a and its corresponding polyMOFs were selected as the primary validation of the DFT calculations, as pbdc-7a displayed the most conformationally relaxed structures in both polyMOF systems. Figure 4 shows nearly quantitative multiCP[32] ^{13}C NMR spectra of pbdc-7a, polyIRMOF-1-7a, and polyUiO-66-7a. Deprotonation and coordination of the carboxylate groups in the polyMOFs results in two pronounced chemical shifts changes, of the carboxylate carbon and of the aromatic carbon labeled C2 (Figure 4) to which it is bonded. The latter change, from 122 to 130 ppm, is well documented for -COOH vs. -COO^- substituents. Whereas polyIRMOF-1-7a shows only these expected chemical-shift changes, polyUiO-66-7a exhibits line broadening and additional signals, indicative of structural heterogeneity due to strain in its backbone. Signal of the free linkers near 122 ppm, while overlapping with aromatic-CH intensity, can be resolved by spectral editing, specifically recoupled dipolar dephasing (Figure 4, thin lines). For polyUiO-66-7a, 89±4% of the bdc^{2-} linkers are Zr-bound, while 7±3% are uncoordinated H_2bdc (COO^-) groups. Another 4±2 % of the linkers are in the form of ethyl esters (-$COOCH_2CH_3$ groups) that are residual protecting groups from the polymer ligand synthesis (signals at 62 and 12 ppm; note these are observed for pbdc-7a and polyIRMOF-1-7a as well). Complex line broadening can be seen in the OCH_2 and aromatic C-O resonances (highlighted by red arrows in Figure 4c).

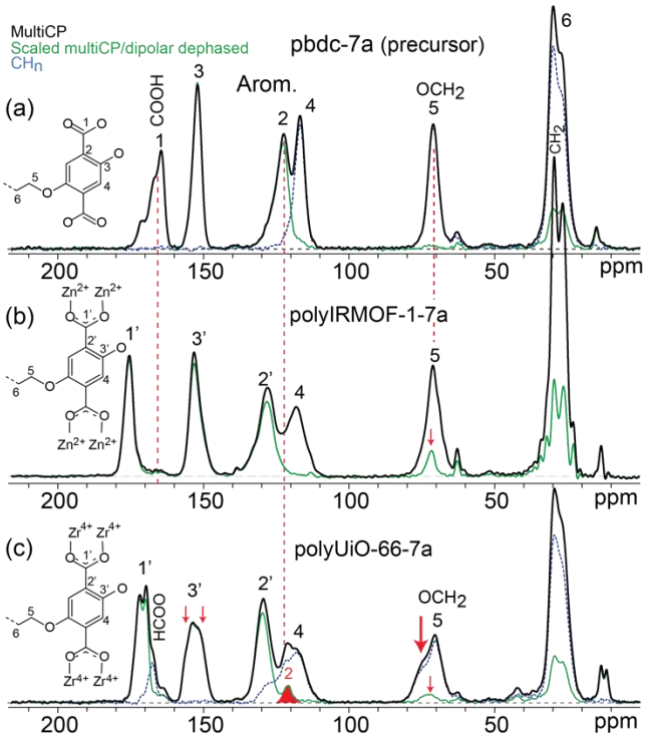

Figure 4. Probing for uncoordinated linkers and strain in polyMOFs with -$(CH_2)_7$- backbone spacer segments by multiCP ^{13}C NMR. Spectra of (a) pbdc-7a, (b) polyIRMOF-1-7a, and (c) polyUiO-66-7a. Thin green lines: spectra of C not bonded to H or mobile segments, obtained after recoupled dipolar dephasing. The resolved residual signal of uncoordinated linkers in (c) is highlighted by shading.

The coordination of linkers in the polyMOFs is associated with deprotonation of the carboxylate groups in pbdc-7a. This protonation change can be detected as a chemical-shift increase of the carboxylate resonance from ~165 to ~170 ppm in the ^{13}C NMR spectrum. It is even clearer in HetCor ^{13}C-^{1}H NMR, where -COOH groups produce distinct resonances at ^{1}H chemical shifts >10 ppm (Figure S29). For polyUiO-66-7a, the HetCor experiment also revealed differences in magnetization transfer from ^{1}H to OCH_2 carbons at 70 ppm (peak) and 75 ppm (shoulder) (Figure S30) indicative of differences in conformation, packing, and/or dynamics.

Strain on the backbone spacer segments in polyMOFs is expected to reduce the amplitudes of their thermal motions in the pores of the MOF lattice. While unselective ^{1}H spectra provide only limited information (Figure S31) wideline separation (WISE) ^{1}H-^{13}C NMR[33] (Figure 5) can probe the amplitudes of fast segmental motions in polyMOFs in terms of motional narrowing of ^{1}H wideline spectra obtained for each resolved ^{13}C peak. In pbdc-7a-derived polyMOFs, the WISE experiment probes mostly the motion of the geminal H-H internuclear vector, which is approximately perpendicular to the local chain axis. In addition, the linewidth also reflects the local ^{1}H density, which decreases progressively from crystalline poly(ε-caprolactone) (which serves as a rigid-limit reference with

-$(CH_2)_5$- units) to pbdc-7a with its proton-poor substituted 1,4-benzenedicarboxylic acid segments, and finally to the polyMOFs with their inorganic nodes and free pore space. Because the proton density is similar in the two polyMOF materials, the significantly smaller line widths of the -OCH_2- and other -CH_2- protons in polyIRMOF-1-7a relative to polyUiO-66-7a (Figure 5) indicate larger-amplitude motions around the local chain axis in polyIRMOF-1-7a. Conversely, this can be described as more constraints on chain motions in the pores of polyUiO-66-7a relative to polyIRMOF-1-7a.

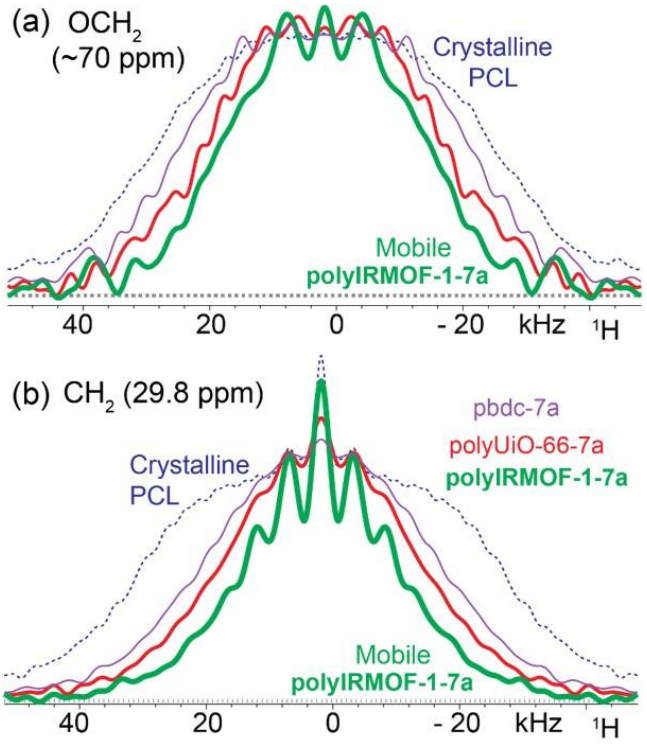

Figure 5. Probing -CH_2- motions and proton density in polyMOFs. ^{1}H wideline spectra of (a) -OCH_2- and (b) other -CH_2- groups in pbdc-7a and its corresponding polyMOFs, obtained as slices at peak maxima near 70 and 29.8 ppm, respectively, from 2D WISE ^{1}H-^{13}C spectra. Dashed lines (blue): crystalline poly(ε-caprolactone), a polyester containing -$(CH_2)_5$- units, shown as the rigid-limit reference; thin lines (purple): pbdc-7a; thick lines (red): polyUiO-66-7a; thickest lines (green): polyIRMOF-1-7a. A smaller line width and the appearance of spinning sidebands can be due to large-amplitude motions of the H-H internuclear vector or a reduced ^{1}H density.

Fast motions can also be probed, without confounding ^{1}H density effects, via the ^{13}C chemical shift anisotropy (CSA). This orientation-dependent interaction is time-averaged to zero by magic-angle spinning but can be "recoupled" by a few rotation-synchronized radio-frequency pulses each with a flip angle of 180°.[34] The larger the motional amplitude, the slower the observed relaxation (dephasing).[34] Data shown in Figure S32 show that the -OCH_2- groups in polyIRMOF-1-7a undergo larger-amplitude motions than those in pbdc-7a or polyUiO-66-7a, in agreement with the WISE NMR data. Taken together, the dynamical NMR experiments consistently document more freedom of motion in polyIRMOF-1-7a, indicating more relaxed backbone chain segments in this polyMOF relative to polyUiO-66-7a.

CONCLUSIONS

In conclusion, structure models for polyIRMOF-1-xa and poly-UiO-66-xa with x = 6, 7, and 8 have been constructed and further geometry-optimized at the DFT level. The chains of polyUiO-66 were found to be much more mechanically constrained than those of polyIRMOF-1. Significant distortions of the -$(CH_2)_x$- segments were predicted for polyUiO-66-6a and may account for a notable amount of uncoordinated bdc^{2-} units detected by ssNMR. The polyIRMOF-1-7a and poly-UiO-66-7a models were further supported by the conclusions drawn using ssNMR. Whereas polyIRMOF-1-7a shows relatively narrow lines in the ssNMR spectra, polyUiO-66-7a exhibits multiple components in some aromatic signals and a pronounced shoulder of the -OCH_2- signal that extends beyond the range typically observed due to different conformers. These are signatures of the chain stretching and structural distortions seen in the DFT calculations. Significantly larger amplitudes of motion around the local chain axes indicate more relaxed, mobile chains in polyIRMOF-1-7a. Signal of residual uncoordinated linkers can be resolved in polyUiO-66-7a but not in polyIRMOF-1-7a. This powerful combination of ssNMR and molecular simulations allows us to unveil the structure and dynamics of polyMOF materials at the atomistic level for the first time. Overall, understanding of the internal structure of polyMOFs is expected to not only aid the design of these hybrid materials but also discover unique properties issued from a synergistic coupling of polymer chains and MOF architectures.

ASSOCIATED CONTENT

Computational details, synthesis and characterization details, ssNMR details, and supporting figures can be found in the Supporting information. This material is available free of charge via the Internet at http://pubs.acs.org.

AUTHOR INFORMATION

Corresponding Authors

*guillaume.maurin1@umontpellier.fr
*srohr@brandeis.edu
*scohen@ucsd.edu

Notes

The authors declare no competing financial interests.

ACKNOWLEDGMENT

SEM imaging was performed at the San Diego Nanotechnology Infrastructure (SDNI) of U.C. San Diego, a member of the National Nanotechnology Coordinated Infrastructure, which is supported by the National Science Foundation (Grant ECCS-1542148). The solid-state NMR spectrometer used in this work was funded by the NSF MRI program (Award No. 1726346). This work was supported by a grant from the Department of Energy, Office of Basic Energy Sciences, Division of Materials Science and Engineering under Award No. DE-FG02-08ER46519. S.A. was supported, in part, by a fellowship from the Department of Education Graduate Assistance in Areas of National Need (GAANN) Training Grant and the Inamori Foundation.

REFERENCES

1. Kalaj, M.; Bentz, K. C.; Ayala, S.; Palomba, J. M.; Barcus, K. S.; Katayama, Y.; Cohen, S. M., MOF-Polymer Hybrid Materials: From Simple Composites to Tailored Architectures. *Chem. Rev.* **2020**, ASAP contents.
2. Kitao, T.; Zhang, Y.; Kitagawa, S.; Wang, B.; Uemura, T., Hybridization of MOFs and polymers. *Chem. Soc. Rev.* **2017,** *46* (11), 3108-3133.
3. Denny, M. S.; Moreton, J. C.; Benz, L.; Cohen, S. M., Metal–organic frameworks for membrane-based separations. *Nat. Rev. Mater.* **2016,** *1* (12), 16078.
4. Zhang, Y.; Feng, X.; Yuan, S.; Zhou, J.; Wang, B., Challenges and recent advances in MOF–polymer composite membranes for gas separation. *Inorg. Chem. Front.* **2016,** *3* (7), 896-909.
5. Zhang, Y.; Feng, X.; Li, H.; Chen, Y.; Zhao, J.; Wang, S.; Wang, L.; Wang, B., Photoinduced Postsynthetic Polymerization of a Metal–Organic Framework toward a Flexible Stand-Alone Membrane. *Angew. Chem. Int. Ed.* **2015,** *54* (14), 4259-4263.
6. Gao, X.; Zhang, J.; Huang, K.; Zhang, J., ROMP for Metal–Organic Frameworks: An Efficient Technique toward Robust and High-Separation Performance Membranes. *ACS Appl. Mater. Interfaces* **2018,** *10* (40), 34640-34645.
7. Nagata, S.; Kokado, K.; Sada, K., Metal–organic framework tethering PNIPAM for ON–OFF controlled release in solution. *Chem. Commun.* **2015,** *51* (41), 8614-8617.
8. Mochizuki, S.; Ogiwara, N.; Takayanagi, M.; Nagaoka, M.; Kitagawa, S.; Uemura, T., Sequence-regulated copolymerization based on periodic covalent positioning of monomers along one-dimensional nanochannels. *Nat. Commun.* **2018,** *9* (1), 329.
9. Uemura, T.; Uchida, N.; Higuchi, M.; Kitagawa, S., Effects of Unsaturated Metal Sites on Radical Vinyl Polymerization in Coordination Nanochannels. *Macromolecules* **2011,** *44* (8), 2693-2697.
10. Uemura, T.; Kitagawa, K.; Horike, S.; Kawamura, T.; Kitagawa, S.; Mizuno, M.; Endo, K., Radical polymerisation of styrene in porous coordination polymers. *Chem. Commun.* **2005,** (48), 5968-5970.
11. Gu, Y.; Huang, M.; Zhang, W.; Pearson, M. A.; Johnson, J. A., PolyMOF Nanoparticles: Dual Roles of a Multivalent polyMOF Ligand in Size Control and Surface Functionalization. *Angew. Chem. Int. Ed.* **2019,** *58* (46), 16676-16681.
12. Hwang, J.; Heil, T.; Antonietti, M.; Schmidt, B. V. K. J., Morphogenesis of Metal–Organic Mesocrystals Mediated by Double Hydrophilic Block Copolymers. *J. Am. Chem. Soc.* **2018,** *140* (8), 2947-2956.
13. Denny Jr., M. S.; Cohen, S. M., In Situ Modification of Metal–Organic Frameworks in Mixed-Matrix Membranes. *Angew. Chem. Int. Ed.* **2015,** *54* (31), 9029-9032.
14. Smith, Z. P.; Bachman, J. E.; Li, T.; Gludovatz, B.; Kusuma, V. A.; Xu, T.; Hopkinson, D. P.; Ritchie, R. O.; Long, J. R., Increasing M2(dobdc) Loading in Selective Mixed-Matrix Membranes: A Rubber Toughening Approach. *Chem. Mater.* **2018,** *30* (5), 1484-1495.
15. Sabetghadam, A.; Seoane, B.; Keskin, D.; Duim, N.; Rodenas, T.; Shahid, S.; Sorribas, S.; Guillouzer, C. L.; Clet, G.; Tellez, C.; Daturi, M.; Coronas, J.; Kapteijn, F.; Gascon, J., Metal Organic Framework Crystals in Mixed-Matrix Membranes: Impact of the Filler Morphology on the Gas Separation Performance. *Adv. Func. Mater.* **2016,** *26* (18), 3154-3163.
16. He, S.; Wang, H.; Zhang, C.; Zhang, S.; Yu, Y.; Lee, Y.; Li, T., A generalizable method for the construction of MOF@polymer functional composites through surface-initiated atom transfer radical polymerization. *Chem. Sci.* **2019,** *10* (6), 1816-1822.
17. Uemura, T.; Horike, S.; Kitagawa, K.; Mizuno, M.; Endo, K.; Bracco, S.; Comotti, A.; Sozzani, P.; Nagaoka, M.; Kitagawa, S., Conformation and Molecular Dynamics of Single Polystyrene Chain Confined in Coordination Nanospace. *J. Am. Chem. Soc.* **2008,** *130* (21), 6781-6788.
18. Uemura, T.; Yanai, N.; Watanabe, S.; Tanaka, H.; Numaguchi, R.; Miyahara, M. T.; Ohta, Y.; Nagaoka, M.; Kitagawa, S., Unveiling thermal transitions of polymers in subnanometre pores. *Nat. Commun.* **2010,** *1* (1), 83.
19. Yanai, N.; Uemura, T.; Kitagawa, S., Behavior of Binary Guests in a Porous Coordination Polymer. *Chem. Mater.* **2012,** *24* (24), 4744-4749.
20. Duan, P.; Moreton, J. C.; Tavares, S. R.; Semino, R.; Maurin, G.; Cohen, S. M.; Schmidt-Rohr, K., Polymer Infiltration into Metal–Organic Frameworks in Mixed-Matrix Membranes Detected in Situ by NMR. *J. Am. Chem. Soc.* **2019,** *141* (18), 7589-7595.
21. Semino, R.; Moreton, J. C.; Ramsahye, N. A.; Cohen, S. M.; Maurin, G., Understanding the origins of metal–organic framework/polymer compatibility. *Chem. Sci.* **2018,** *9* (2), 315-324.
22. Zhang, Z.; Nguyen, H. T. H.; Miller, S. A.; Cohen, S. M., polyMOFs: A Class of Interconvertible Polymer-Metal-Organic-Framework Hybrid Materials. *Angew. Chem. Int. Ed.* **2015,** *54* (21), 6152-6157.
23. Schukraft, G. E. M.; Ayala, S.; Dick, B. L.; Cohen, S. M., Isoreticular expansion of polyMOFs achieves high surface area materials. *Chem. Commun.* **2017,** *53* (77), 10684-10687.
24. Ayala, S.; Zhang, Z.; Cohen, S. M., Hierarchical structure and porosity in UiO-66 polyMOFs. *Chem. Commun.* **2017,** *53* (21), 3058-3061.
25. Ayala, S.; Bentz, K. C.; Cohen, S. M., Block co-polyMOFs: morphology control of polymer–MOF hybrid materials. *Chem. Sci.* **2019,** *10* (6), 1746-1753.
26. Palomba, J. M.; Ayala Jr., S.; Cohen, S. M., polyMOF Formation from Kinked Polymer Ligands via ortho-Substitution. *Isr. J. Chem.* **2018,** *58* (9-10), 1123-1126.
27. MacLeod, M. J.; Johnson, J. A., Block co-polyMOFs: assembly of polymer–polyMOF hybrids via iterative exponential growth and "click" chemistry. *Polym. Chem.* **2017,** *8* (31), 4488-4493.
28. Zhang, Z.; Nguyen, H. T. H.; Miller, S. A.; Ploskonka, A. M.; DeCoste, J. B.; Cohen, S. M., Polymer–Metal–Organic Frameworks (polyMOFs) as Water Tolerant Materials for Selective Carbon Dioxide Separations. *J. Am. Chem. Soc.* **2016,** *138* (3), 920-925.

29. Perdew, J. P.; Burke, K.; Ernzerhof, M., Generalized Gradient Approximation Made Simple. *Phys. Rev. Lett.* **1996,** *77* (18), 3865-3868.
30. Grimme, S.; Antony, J.; Ehrlich, S.; Krieg, H., A consistent and accurate ab initio parametrization of density functional dispersion correction (DFT-D) for the 94 elements H-Pu. *J. Chem. Phys.* **2010,** *132* (15), 154104.
31. Hutter, J.; Iannuzzi, M.; Schiffmann, F.; VandeVondele, J., cp2k: atomistic simulations of condensed matter systems. *Comput. Mol. Sci.* **2014,** *4* (1), 15-25.
32. Duan, P.; Schmidt-Rohr, K., Composite-pulse and partially dipolar dephased multiCP for improved quantitative solid-state 13C NMR. *J. Magn. Reson.* **2017,** *285*, 68-78.
33. Schmidt-Rohr, K.; Clauss, J.; Spiess, H. W., Correlation of structure, mobility, and morphological information in heterogeneous polymer materials by two-dimensional wideline-separation NMR spectroscopy. *Macromolecules* **1992,** *25* (12), 3273-3277.
34. Mao, J. D.; Schmidt-Rohr, K., Separation of aromatic-carbon 13C NMR signals from di-oxygenated alkyl bands by a chemical-shift-anisotropy filter. *Solid State Nucl. Magn. Reson.* **2004,** *26* (1), 36-45.

TOC Graphic

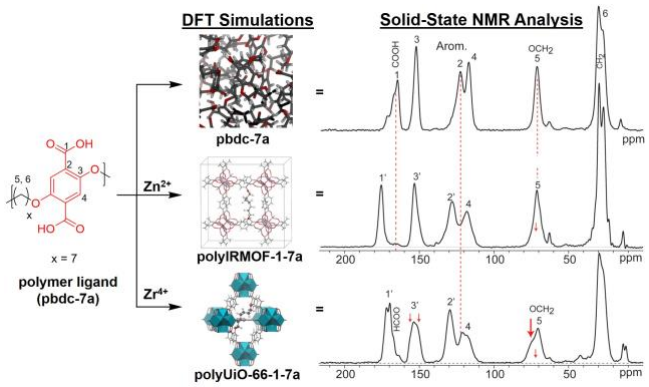
DFT Simulations
Solid-State NMR Analysis
pbdc-7a
polyIRMOF-1-7a
polyUiO-66-1-7a
polymer ligand
(pbdc-7a)
x = 7
Zn2+
Zr4+
COOH
Arom.
OCH2
CH2
HCOO
ppm
200
150
100
50